Design and Adaptive Depth Control of a Micro Diving Agent

Wallace M. Bessa, Edwin Kreuzer, Johann Lange, Marc-André Pick, and Eugen Solowjow

***Abstract*—This letter presents the depth control of an autonomous micro diving agent called autonomous diving agent (ADA). ADA consists of off-the-shelf components and features open-source hardware and firmware. It can be deployed as a testbed for depth controllers, as well as a mobile sensor platform for research or in industrial tanks. We introduce a control law that is based on the feedback linearization method and enhanced by an adaptive fuzzy algorithm to cope with modeling inaccuracies. The proposed depth controller is computationally light enough to run on ADAs embedded hardware. In experiments performed in a wave tank, the adaptive fuzzy scheme shows the ability to deal with both depth regulation and depth profile tracking. ADA is even able to hold on to dynamic isobars despite external disturbances. We demonstrate that under the influence of waves, ADA describes orbital motions similar to water particles.**

***Index Terms*—Fuzzy control, marine robotics, mechanism design, robust/adaptive control of robotic systems.**

I. Introduction

In THE last decades underwater robotic systems have been widely employed for ocean monitoring and exploration [1]–[3]. Both, remotely operated and autonomous underwater vehicles are commonly used to gather marine data.

In addition to conventional underwater robots, great attention has recently also been paid to the improvement of profiling floats [4]–[6] and to the development of underwater sensor networks [7], [8]. As a matter of fact, small underwater agents can be deployed for exploring ocean phenomena with different spatial and temporal scales [4], [9]. Due to their compact size, they can be considered as hydrodynamically transparent and can depict almost a Lagrangian representation of the fluid flow, which makes them an adequate instrument for studying submesoscale processes [9]. Furthermore, micro diving robots can be deployed in confined industrial tanks, e. g. for monitoring chemical processes. When equipped with appropriate sensors, they can provide measurements of temperature, pH-values, or some desired chemical concentration [10]. On this basis, it should be emphasized that, since the vertical gradients in liquids are most pronounced, diving agents must be able to precisely follow a specific depth profile.

Another important aspect is related to the research of orbital motions resulting from surface waves. Water particles move on orbitals under the influence of surface gravity waves [11]. These orbitals are usually visualized by laborious optical methods. A small submerged body that is stabilized on an isobar exhibits dynamics similar to those of surrounding water particles and could be used to facilitate the investigation of orbital motions [12].

A common issue involving underwater robots concerns depth control. While there is a growing body of depth control literature, the problem remains in the realm of active research [13]–[17]. Depth regulation resembles the inverted pendulum stabilization problem, because in both cases the desired state is an unstable equilibrium point. As in many other application areas, PID control is the most common approach [4], [9], [13]. However, PID and other linear controllers can in general not guarantee accurate tracking performance [9], [16]. Inherently nonlinear dynamics, uncertain hydrodynamic coefficients, and external disturbances, render precise dynamic positioning of autonomous marine systems very challenging [18]. Thus, in order to cope with the nonlinear terms and external disturbances, feedback linearization with phase lead compensation was proposed for Lagrangian profiling floats in [16].

Variable structure methods have been extensively studied for depth control. Sliding mode approaches, for example, can confer robustness to both model uncertainties and external disturbances [19]. However, sliding mode controllers are often subject to undesired chattering effects. A common approach for reducing chattering is the adoption of a thin boundary layer neighboring the switching surface [20], but it also introduces a steady-state error. Therefore, intelligent control schemes gained a lot of interest for depth control [12], [17], since they combine the advantages of nonlinear control techniques, while enhancing the tracking performance.

This letter contributes a novel adaptive fuzzy feedback linearization (AFFL) scheme for depth control. Moreover, we demonstrate its implementation on a compact micro diving robot

Manuscript received February 15, 2017; accepted May 31, 2017. Date of publication June 9, 2017; date of current version June 21, 2017. This letter was recommended for publication by Associate Editor M. D. Dunbabin and Editor J. Roberts upon evaluation of the reviewers' comments. This work was supported by the German Research Foundation under Grant Kr 752/33-1. The work of W. M. Bessa was supported in part by the Alexander von Humboldt Foundation and in part by the Brazilian Coordination for the Improvement of Higher Education Personnel. *(Corresponding author: Eugen Solowjow.)*

W. M. Bessa is with the Institute of Mechanics and Ocean Engineering, Hamburg University of Technology, Hamburg 21073, Germany, on leave from the Department of Mechanical Engineering, Federal University of Rio Grande do Norte, Natal, Brazil (e-mail: wmbessa@ct.ufrn.br).

E. Kreuzer, J. Lange, M.-A. Pick, and E. Solowjow are with the Institute of Mechanics and Ocean Engineering, Hamburg University of Technology, Hamburg 21073, Germany (e-mail: kreuzer@tuhh.de; johann.lange@tuhh.de; pick@tuhh.de; eugen.solowjow@tuhh.de).

This paper has supplementary downloadable material available at http://ieeexplore.ieee.org.

Color versions of one or more of the figures in this paper are available online at http://ieeexplore.ieee.org.

Digital Object Identifier 10.1109/LRA.2017.2714142

Fig. 1. Micro diving agent ADA.

called ADA (Autonomous Diving Agent). ADA, which is shown in Fig. 1, is equipped with a pressure and temperature sensor, a microcontroller board, and an actuation mechanism for adjusting buoyancy. It can be deployed for studying small-scale phenomena from a Lagrangian perspective, as a monitoring system in industrial tanks, and also as a testbed for new control concepts in research and education. The version of ADA presented in this letter is designed for depths of up to 10 m. While the housing could withstand pressures of up to 100 m, the installed motor lacks power to displace volume at those depths. However, a more powerful motor can be installed with only minor design changes.

The depth control approach is computationally light so that it can be implemented on ADA's embedded hardware. This is achieved by designing the adopted inference system of the control law with only a single input variable, which significantly reduces the number of fuzzy sets and rules. The boundedness and convergence properties of the closed-loop signals are analytically proven. The performance has been experimentally evaluated in a wave tank, where it outperforms a conventional feedback linearization controller. The proposed controller is easy to tune, and is able to provide not only depth holding but also accurate depth profile tracking, despite unmodeled dynamics. Based on the capability to stabilize itself on an isobar, we show that ADA is able to follow orbital trajectories too.

This letter is organized as follows. The system design is described in Section III. Section IV outlines the nonlinear control strategy for depth control. Section V presents the experimental results for depth holding, depth profile tracking, and orbital motion under the influence of surface waves. The concluding remarks are presented in Section V.

II. System Design

ADA is able to change its buoyancy by adjusting the displaced volume, which results in rising or sinking. Accordingly, actuator design is an important part of the system design. The actuation system has to react quickly and the overall change of volume should be as large as possible to yield high forces. Other main design specifications include compactness and

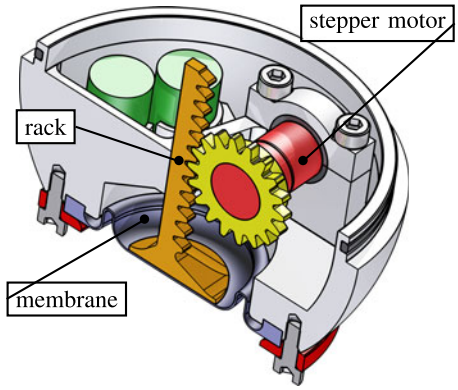

Fig. 2. Rendered CAD model of actuation components.

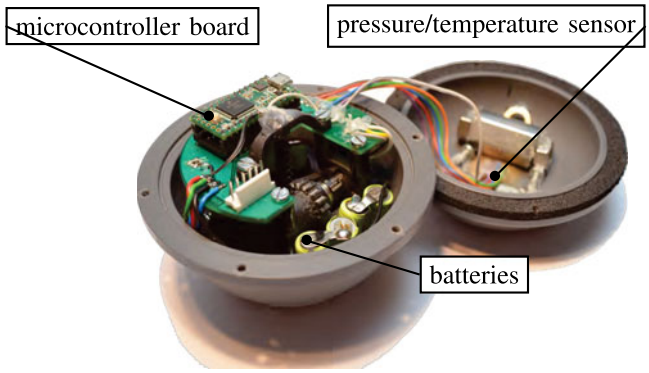

Fig. 3. Components of ADA.

off-the-shelf components. The firmware design follows a low-level procedural paradigm resulting in a small footprint.

A. Hardware Design

The volume of ADA is dynamically changed by means of a rubber membrane, which also seals the system. The membrane can travel up to 15 mm in each direction and is actuated by a stepper motor via a rack and a pinion. The membrane displaces a total volume of 9817 mm^3, which is equivalent to $\pm 2.75\%$ of the total volume. A complete change of the buoyancy volume from -2.75% to 2.75% takes 0.46 s at a depth of 1 m. For increasing depth, the time it takes to change the volume increases. The actuation resolution is 6 mm^3, or 0.0033% of ADAs total volume. In Fig. 2 the actuation mechanism is shown as a rendered image with the membrane depicted in purple.

The assembly of ADA can be seen in Fig. 3 with the Teensy microcontroller board on the top left and the actuator mechanism in black in the middle of the lower shell. The actuation mechanism and the inside structure are mostly 3D printed. In the background, the upper shell of ADA is shown with the wires routed to the pressure and temperature sensor AMSYS MS5803 which is embedded in the housing and interfaced via SPI.

Different sensor versions with the same form factor are available for pressures of up to 14 bar which corresponds to approximately 140 m water depth. The sensor family provides depth resolutions of two millimeters for the 14 bar version and less

than one millimeter for the other versions. The temperature resolution is $< 0.01\,^{\circ}\mathrm{C}$ and the temperature range is $-40\,^{\circ}\mathrm{C}$ to $+85\,^{\circ}\mathrm{C}$.

The presented version of ADA is powered by NiMh batteries. The operational time depends on the depth. At 1 m depth the operational time is approximately 20 min with a battery capacity of 170 mAh. A LiPo battery with 1200 mAh and 2 h operational time can be included for a slightly modified arrangement of the inner components without any changes to the overall volume.

B. Firmware Design

The firmware is customized for the Teensy microcontroller board and is written in C++. The firmware is open source and can be obtained at https://github.com/JohannLange/ADA_AFFL. The control law is implemented following a procedural programming paradigm and is implemented within a low-level loop. The main functions consist of pressure and temperature sensor queries for determining water depth, control command computations and stepper motor actuation. The main loop runs at 40 Hz. Data is logged at a frequency of 2 Hz and stored in EEPROM.

III. Depth Control System

High control performance usually requires an accurate plant model, which in practice can be very difficult to obtain. Especially in the case of a diving agent, its equation of motion should not only take rigid body effects into account, but also precisely represent the interaction with the surrounding fluid and the actuator dynamics. Although the Navier-Stokes equations could be used to describe fluid-rigid body interaction, it would not be proper for real-time control.

The adoption of a lumped parameters approach to estimate the hydrodynamic effects, on the other hand, depends on the estimation of empirical coefficients. These coefficients vary depending on different flow conditions [21]. The choice of constant coefficients for all conditions oversimplifies the fluid-body interaction in this application.

In this work a different approach is adopted. Here, only the dynamical effects that can be estimated exactly and in a straightforward manner are taken into account for the development of the control law. In order to automatically recognize the unmodeled dynamics and compensate for it, an adaptive fuzzy inference system is additionally embedded in the control law.

Since gravity and buoyancy effects can be accurately modelled, only these restoring forces are incorporated in the balance of forces:

$$m\ddot{z} = F_{\mathrm{G}} - F_{\mathrm{B}} = mg - \rho g \nabla, \tag{1}$$

with m being the mass of the diving agent, z representing its depth position, F_{G} and F_{B} the gravity and buoyancy forces, respectively, g the gravitational acceleration, ρ the water density, and ∇ the displaced volume of fluid. It should be also noted that the z-axis is pointing downwards.

If the volume corresponding to zero buoyancy is represented by v_0, then the displaced volume can be conveniently adjusted by means of the mechanism described in Section II, $\nabla = v_0 + v$, in order to regulate the depth of the diving agent. However, since the actuator dynamics can not be neglected, a first-order low pass filter is adopted to represent its behavior

$$\dot{v} = -\alpha(v - u), \tag{2}$$

where u is the control signal and α is a strictly positive parameter related to the filter time constant.

Now, with the aim to design the control law, (2) is combined with the time derivative of (1), leading to a third-order differential equation that represents the dynamical behavior of the diving agent:

$$m\dddot{z} = \alpha\rho g(v - u) + d\,, \tag{3}$$

with d being added to the model in order to represent neglected dynamical effects.

The proposed control problem is to ensure that, even in the presence of unmodeled dynamics, the state vector $\boldsymbol{z} = [z\ \dot{z}\ \ddot{z}]^{\top}$ will follow a desired state $\boldsymbol{z}_{\mathrm{d}} = [z_{\mathrm{d}}\ \dot{z}_{\mathrm{d}}\ \ddot{z}_{\mathrm{d}}]^{\top}$, i. e., the error vector $\tilde{\boldsymbol{z}} = [\tilde{z}\ \dot{\tilde{z}}\ \ddot{\tilde{z}}]^{\top} = [z - z_{\mathrm{d}}\ \dot{z} - \dot{z}_{\mathrm{d}}\ \ddot{z} - \ddot{z}_{\mathrm{d}}]^{\top} \rightarrow \mathbf{0}$ as $t \rightarrow \infty$.

Thus, following the feedback linearization method, the control law is defined as

$$u = \frac{1}{\alpha\rho g}\Big[\alpha\rho g v - m(\dddot{z}_{\mathrm{d}} - 3\lambda\ddot{\tilde{z}} - 3\lambda^2\dot{\tilde{z}} - \lambda^3\tilde{z}) + \hat{d}\Big], \tag{4}$$

with λ being a strictly positive constant and $\hat{d}$ representing an estimate of d.

By applying the proposed controller (4) to the diving agent (3), the closed-loop dynamics can be expressed by

$$\dddot{\tilde{z}} + 3\lambda\ddot{\tilde{z}} + 3\lambda^2\dot{\tilde{z}} + \lambda^3\tilde{z} = m^{-1}(d - \hat{d}). \tag{5}$$

It can be easily verified from (5) that in the ideal case, i. e., either the plant dynamics or $\hat{d} = d$ are perfectly known, the error vector converges exponentially to zero. Otherwise, the tracking error will be driven by the approximation error.

Considering that fuzzy logic can be used to approximate the neglected dynamical effects with an arbitrary degree of accuracy [22]: $d = \hat{d}^{*} + \varepsilon$, with $\hat{d}^{*}$ being the optimal estimate and ε the minimum approximation error, a TSK (Takagi–Sugeno–Kang) inference system is adopted as a universal approximator:

$$\hat{d} = \widehat{\boldsymbol{D}}^{\top}\boldsymbol{\Psi}\,, \tag{6}$$

where $\widehat{\boldsymbol{D}} = [\widehat{D}_1\ \widehat{D}_2\ \ldots\ \widehat{D}_n]^{\top}$ is a vector containing the attributed values to each fuzzy rule, $\boldsymbol{\Psi} = [\psi_1\ \psi_2\ \ldots\ \psi_n]^{\top}$, with $\psi_i = w_i / \sum_{i=1}^{n} w_i$, and w_i being the firing strength of each rule.

In order to simplify the design process and to avoid the drawbacks related to the curse of dimensionality [23], this work considers only one single variable in the premise of the fuzzy rules. Hence, a combined error measure inspired by the sliding mode method is adopted:

$$\sigma = \ddot{\tilde{z}} + 2\lambda\dot{\tilde{z}} + \lambda^2\tilde{z}\,. \tag{7}$$

On this basis, the closed-loop dynamics (5) can be conveniently rewritten as

$$\dot{\sigma} + \lambda\sigma = m^{-1}(d - \hat{d}). \tag{8}$$

The boundedness of the closed-loop signals and the convergence properties of the tracking error can be investigated by means of a Lyapunov-like stability analysis. Thus, Let a positive-definite function V be defined as

$$V(t) = \frac{1}{2}\sigma^2 + \frac{1}{2\bar{\varphi}}\boldsymbol{\Delta}^\top\boldsymbol{\Delta}\,, \tag{9}$$

with $\boldsymbol{\Delta} = \widehat{\boldsymbol{D}} - \widehat{\boldsymbol{D}}^*$, $\widehat{\boldsymbol{D}}^*$ being the optimal parameter vector, associated to the optimal estimate $\hat{d}^*$, and $\bar{\varphi}$ a strictly positive constant.

Considering that $\dot{\boldsymbol{\Delta}} = \dot{\widehat{\boldsymbol{D}}}$, the time derivative of V is

$$\begin{aligned}\dot{V}(t) &= \sigma\dot{\sigma} + \bar{\varphi}^{-1}\boldsymbol{\Delta}^\top\dot{\widehat{\boldsymbol{D}}}\\ &= -[\lambda\sigma - m^{-1}(d-\hat{d})]\sigma + \bar{\varphi}^{-1}\boldsymbol{\Delta}^\top\dot{\widehat{\boldsymbol{D}}}\\ &= -[\lambda\sigma - m^{-1}(\hat{d}^* + \varepsilon - \hat{d})]\sigma + \bar{\varphi}^{-1}\boldsymbol{\Delta}^\top\dot{\widehat{\boldsymbol{D}}}\\ &= -[\lambda\sigma - m^{-1}\varepsilon + m^{-1}(\hat{d}-\hat{d}^*)]\sigma + \bar{\varphi}^{-1}\boldsymbol{\Delta}^\top\dot{\widehat{\boldsymbol{D}}}\\ &= -(\lambda\sigma - m^{-1}\varepsilon + m^{-1}\boldsymbol{\Delta}^\top\boldsymbol{\Psi})\sigma + \bar{\varphi}^{-1}\boldsymbol{\Delta}^\top\dot{\widehat{\boldsymbol{D}}}\\ &= -(\lambda\sigma - m^{-1}\varepsilon)\sigma + \bar{\varphi}^{-1}\boldsymbol{\Delta}^\top(\dot{\widehat{\boldsymbol{D}}} - m^{-1}\bar{\varphi}\sigma\boldsymbol{\Psi}).\end{aligned} \tag{10}$$

Since both m and $\bar{\varphi}$ have positive values, they can be combined into a single adaptation rate $\varphi = m^{-1}\bar{\varphi}$.

Thus, by updating $\widehat{\boldsymbol{D}}$ according to

$$\dot{\widehat{\boldsymbol{D}}} = \varphi\sigma\boldsymbol{\Psi}\,, \tag{11}$$

the time derivative of V becomes

$$\begin{aligned}\dot{V}(t) &= -(\lambda\sigma - m^{-1}\varepsilon)\sigma\\ &\le -(\lambda|\sigma| - \epsilon)|\sigma|,\end{aligned} \tag{12}$$

with $\epsilon \ge m^{-1}|\varepsilon|$ being an upper bound related to the approximation error.

From (12), it can be concluded that $\dot{V}$ is negative semi-definite only when $|\sigma| > \epsilon/\lambda$, which means that with (11) the bound on $\|\widehat{D}\|$ cannot be ensured when $|\sigma| \le \epsilon/\lambda$. However, in order to overcome this issue, the projection algorithm [24] can be adopted to guarantee that $\widehat{D}$ always remains within a convex region $\mathcal{D} = \{\widehat{D} \in \mathbb{R}^n \mid \widehat{D}^\top\widehat{D} \le \delta^2\}$:

$$\dot{\widehat{\boldsymbol{D}}} = \begin{cases} \varphi\sigma\boldsymbol{\Psi} & \text{if } \|\widehat{\boldsymbol{D}}\|_2 < \delta \text{ or}\\ & \text{if } \|\widehat{\boldsymbol{D}}\|_2 = \delta \text{ and } \varphi\sigma\widehat{\boldsymbol{D}}^\top\boldsymbol{\Psi} \le 0\\ \left(I - \frac{\widehat{\boldsymbol{D}}\widehat{\boldsymbol{D}}^\top}{\widehat{\boldsymbol{D}}^\top\widehat{\boldsymbol{D}}}\right)\varphi\sigma\boldsymbol{\Psi} & \text{otherwise,}\end{cases} \tag{13}$$

with δ representing the desired upper bound for $\|\widehat{\boldsymbol{D}}\|_2$.

Hence, by choosing (13) along with $\|\widehat{\boldsymbol{D}}(0)\|_2 \le \delta$, it follows that $|\sigma(t)| \le \epsilon/\lambda$ and $\|\widehat{\boldsymbol{D}}(t)\|_2 \le \delta$ as $t \to \infty$.

From (7), $|\sigma(t)| \le \epsilon/\lambda$ may be rewritten as

$$-\frac{\epsilon}{\lambda} \le \ddot{\tilde{z}} + 2\lambda\dot{\tilde{z}} + \lambda^2\tilde{z} \le \frac{\epsilon}{\lambda}\,. \tag{14}$$

Multiplying (14) by $e^{\lambda t}$ yields

$$-\frac{\epsilon}{\lambda}e^{\lambda t} \le \frac{\mathrm{d}^2}{\mathrm{d}t^2}(\tilde{z}e^{\lambda t}) \le \frac{\epsilon}{\lambda}e^{\lambda t}\,. \tag{15}$$

Integrating (15) between 0 and t gives

$$-\frac{\epsilon}{\lambda^2}e^{\lambda t} + \frac{\epsilon}{\lambda^2} \le \frac{\mathrm{d}}{\mathrm{d}t}(\tilde{z}e^{\lambda t}) - \frac{\mathrm{d}}{\mathrm{d}t}(\tilde{z}e^{\lambda t})\Big|_{t=0} \le \frac{\epsilon}{\lambda^2}e^{\lambda t} - \frac{\epsilon}{\lambda^2}\,, \tag{16}$$

or conveniently rewritten as

$$-\frac{\epsilon}{\lambda^2}e^{\lambda t} - \kappa_1 \le \frac{\mathrm{d}}{\mathrm{d}t}(\tilde{z}e^{\lambda t}) \le \frac{\epsilon}{\lambda^2}e^{\lambda t} + \kappa_1\,, \tag{17}$$

with $\kappa_1 = \epsilon\lambda^{-2} + \dot{\tilde{z}}(0) + \lambda\tilde{z}(0)$ being a constant value.

Integrating (17) between 0 and t gives

$$-\frac{\epsilon}{\lambda^3}e^{\lambda t} - \kappa_1 t - \kappa_0 \le \tilde{z}e^{\lambda t} \le \frac{\epsilon}{\lambda^3}e^{\lambda t} + \kappa_1 t + \kappa_0\,, \tag{18}$$

with $\kappa_0 = \epsilon\lambda^{-3} + \tilde{z}(0)$.

Dividing (18) by $e^{\lambda t}$, it can be verified, for $t \to \infty$, that

$$-\frac{\epsilon}{\lambda^3} \le \tilde{z} \le \frac{\epsilon}{\lambda^3}\,. \tag{19}$$

Applying (19) to (17) and dividing it by $e^{\lambda t}$, it follows, for $t \to \infty$, that

$$-2\frac{\epsilon}{\lambda^2} \le \dot{\tilde{z}} \le 2\frac{\epsilon}{\lambda^2}\,. \tag{20}$$

Furthermore, by imposing (19) and (20) to (14), one has

$$-6\frac{\epsilon}{\lambda} \le \ddot{\tilde{z}} \le 6\frac{\epsilon}{\lambda}\,. \tag{21}$$

Therefore, the proposed controller defined by (4), (6), and (13) ensures the exponential convergence of the tracking error to the closed region $\mathcal{Z} = \left\{\tilde{\boldsymbol{z}} \in \mathbb{R}^3 \;\middle|\; |\tilde{z}^{(i)}| \le (i+1)!\lambda^{i-3}\epsilon\,,\ i = 0,1,2\right\}$.

It must be noted that the proposed control scheme provides a smaller tracking error compared to the conventional feedback linearization approach. By setting the output of the fuzzy inference system to zero, $\hat{d} = 0$, (8) implies that the resulting bounds are $|\tilde{z}^{(i)}| \le (i+1)!\,m^{-1}\lambda^{i-3}|d|\,,\ i = 0,1,2$. Considering that $\epsilon \ll m^{-1}|d|$, from the universal approximation feature of $\hat{d}$, it can be concluded that the tracking error obtained with the adaptive fuzzy feedback linearization scheme is much smaller than the one associated with the conventional approach.

Finally, it is important to emphasize that the adoption of only one single variable as input to the fuzzy inference system not only simplifies the resulting control law, but also avoids the issues related to the curse of dimensionality. For example, if the three error variables ($\tilde{z}$, $\dot{\tilde{z}}$, $\ddot{\tilde{z}}$) had been adopted, instead of the combined error measure σ, the number of fuzzy rules, as well as the adaptive laws that have to be integrated at each time step, would grow from n to n^3 in (11). Keeping computational complexity low makes the proposed approach suitable for ADA's embedded hardware.

IV. Experimental Results

This section presents three different experiments to validate the performance of the ADA platform and the adaptive fuzzy feedback linearization (AFFL) scheme. All trials were carried out in the wave tank of the Institute of Mechanics and Ocean Engineering, Hamburg University of Technology, Fig. 4.

Fig. 4. Wave tank at the Institute of Mechanics and Ocean Engineering, Hamburg University of Technology.

The first experiment consists of a depth holding task with a fixed setpoint. The second experiment is profile tracking of a sinusoidal depth trajectory. In both cases, the AFFL controller is compared with a conventional feedback linearization scheme ($\hat{d} = 0$) in order to demonstrate the efficacy of the adopted adaptive fuzzy algorithm. The third experiment demonstrates the systems ability to lock to an isobar despite external disturbances. This allows ADA to perform orbital motions under the influence of surface waves, in a similar way water particles do.

It should be noted that the proposed controller requires full state feedback. In this case, the depth z can be directly computed from the measured pressure. The other states, namely $\dot{z}$ and $\ddot{z}$, are estimated from z using a conventional sliding mode observer [25]. All details and parameters related to observer and controller are available at https://github.com/JohannLange/ADA_AFFL.

A. Depth Holding

For the depth holding experiment, a reference depth of 0.25 m is set. In Fig. 5 the obtained results are shown for four independent trials.

Both controllers, the adaptive fuzzy and the conventional, are able to reach the setpoint within a reasonable time of approximately 10 sec. However, due to the ability of the AFFL controller to quickly recognize and compensate for unmodeled dynamics (e. g. hydrodynamical effects), the AFFL scheme demonstrates a much smaller steady-state-error.

B. Depth Profile Tracking

In the second experiment the system is tasked to track a sinusoidal depth trajectory. This is a useful behavior for a sensor platform that is supposed to monitor environmental values in a liquid column. The underlying sinusoid of the depth trajectory has an amplitude of 0.2 m and a period of 30 sec. Fig. 6 shows the related results for four independent trials.

The system responses obtained with the AFFL controller are clearly superior to the performance of the conventional FL controller.

The phase portraits of the tracking error related to both controllers allow further analyses. The phase portrait for the conventional approach is shown in Fig. 8 and the tracking error for the AFFL scheme in Fig. 7 The desired state error is

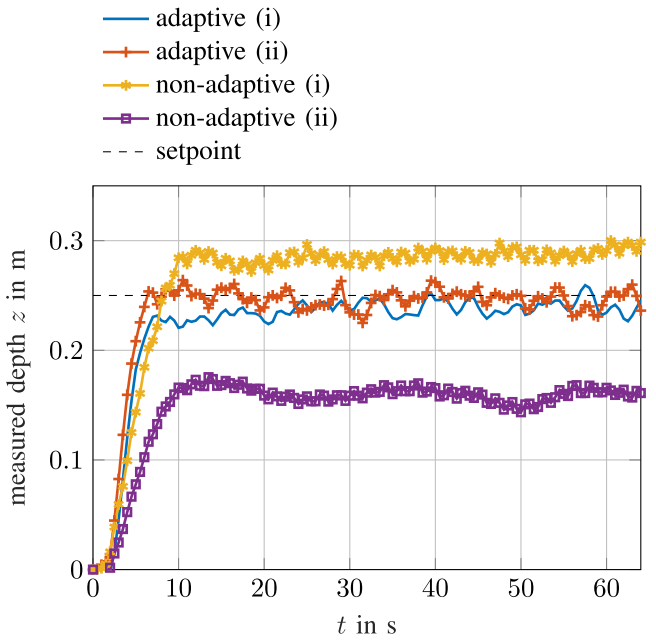

Fig. 5. Depth regulation with both conventional and proposed adaptive control approaches.

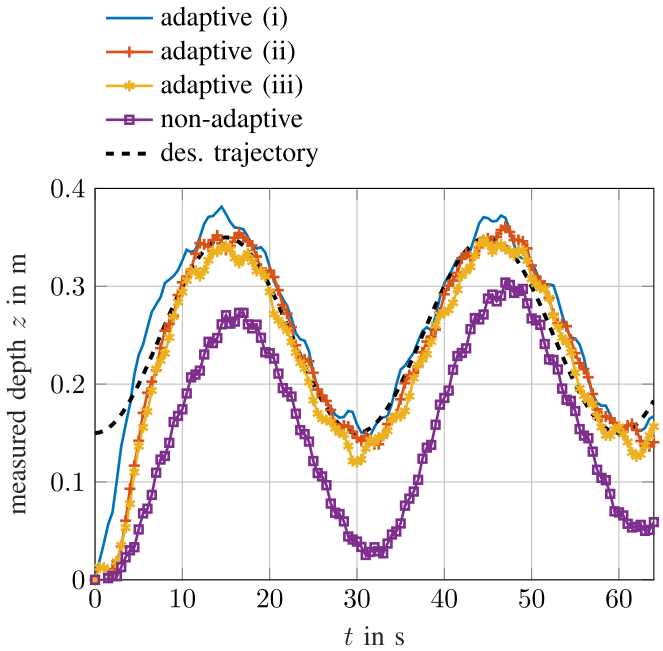

Fig. 6. Depth tracking of a sinusoidal trajectory with conventional FL and proposed AFFL control approaches.

represented by a $\odot$ in the origin. A comparison of both phase portraits reveals that the AFFL controller is able to stabilize the tracking error dynamics around the origin. The conventional FL approach drives the error dynamics towards an undesired fixed point and the overall perturbations of the error dynamics are larger as well. From Figs. 8 and 7, it can also be estimated that $|d| \leq 0.05$ and $|\varepsilon| \leq 0.01$, which means that the adaptive fuzzy inference system is able to compensate for approx. 80% of the modeling inaccuracies.

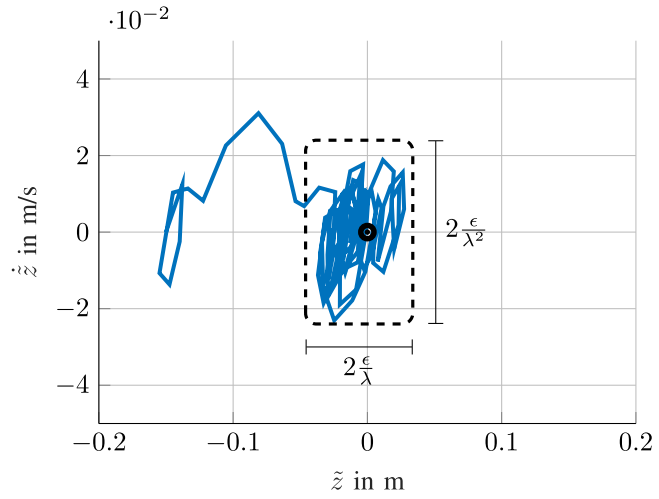

Fig. 7. Phase portrait of the tracking error with the adaptive fuzzy scheme.

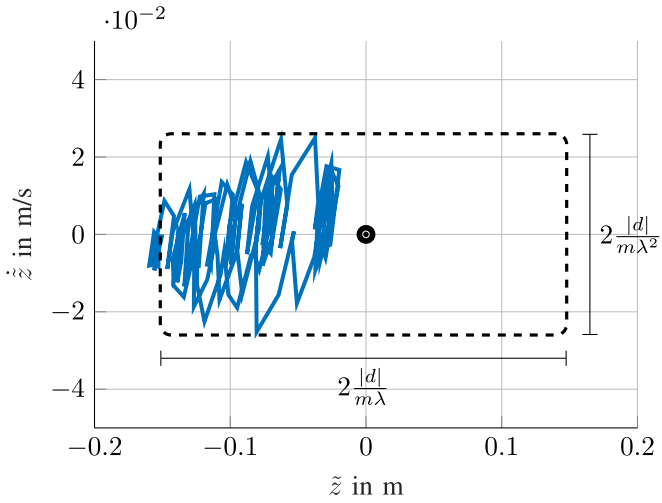

Fig. 8. Phase portrait of the tracking error with the conventional approach.

C. Uncertainty Compensation and Control Energy Analyses

The estimate of the unmodeled dynamics $\hat{d}$ can be reconstructed for the AFFL control trials. However, $\hat{d}$ in time domain resembles colored noise and is of limited use.

The one-sided amplitude spectrum in the frequency domain offers important insights for $\hat{d}$ and is illustrated in Fig. 9 for a representative depth holding and a sinusoidal trajectory tracking experiment. The signals contain unmodeled dynamics, otherwise their spectrums would be flat like the spectrum of white noise. For both data sets most energy is contained below 0.5 Hz with a mode at around 0.4 Hz. In trajectory tracking another mode is present at 0.033 Hz, which is exactly the frequency of the sinusoid to be tracked. Since $\hat{d}$ enters the controls u additively, the AFFL scheme adapts by including the trajectory harmonic in the control signal.

For analyzing the control energy it is important to note, that the fluid force acting on the membrane hardly changes. Thus, the amount of energy required to hold a constant displacement

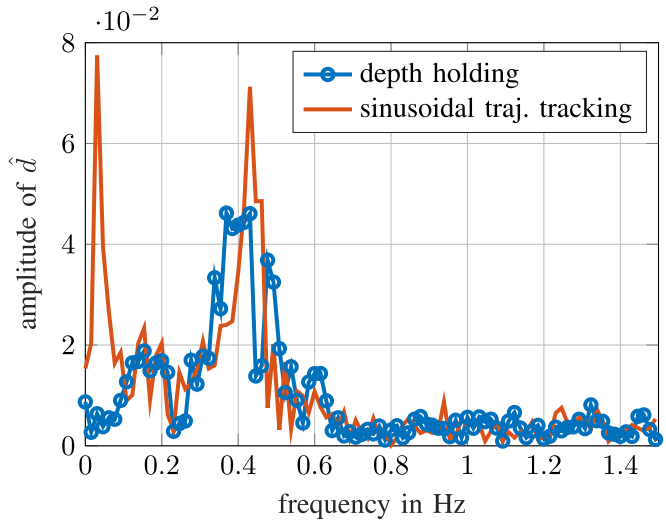

Fig. 9. One-sided amplitude spectrum of $\hat{d}$ for depth tracking of a sinusoidal trajectory and depth holding.

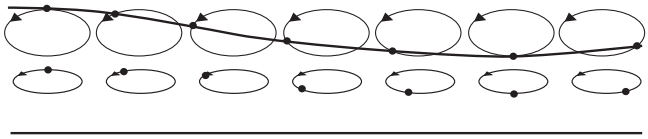

Fig. 10. Trajectories of water particles for two different depths subject to surface waves.

is neglectable. The displacement speed, which is directly linked to the angular velocity of the motor, mainly determines the energy expenditure. Moreover, rotational energy at the motor shaft is proportional to its squared angular velocity. We use this relationship to analyze the spent energy of the AFFL and the FL controllers for the trials depicted in Figs. 5 and 6 by defining the dimensionless quantity

$$E = \int_0^{t_{\text{end}}} \dot{\gamma}^2 \, \mathrm{d}t \,, \tag{22}$$

where γ is the angle of the motor that can be measured by the motor controller. Evaluating (22) and averaging the depth regulation trials yields $\bar{E}_{\text{AFFL,reg}} = 26.06$ and $\bar{E}_{\text{FL,reg}} = 26.54$ for the AFFL and FL controllers, respectively. For sinusoidal trajectory tracking averaged (22) yields $\bar{E}_{\text{AFFL,sin}} = 26.32$ and $\bar{E}_{\text{FL,sin}} = 26.09$, respectively. Therefore, even requiring a similar amount of energy when compared with the conventional approach, the proposed AFFL scheme has a significantly better performance.

D. Orbital Motion Under Surface Water Waves

For harmonic water surface waves linear wave theory dictates that water particles carry out oscillations about fixed points [21]. Their trajectories describe ellipses which become smaller with increasing depth, as illustrated in Fig. 10. The isobars in water are ellipses as well. Hence, a body that can maintain itself on an isobar despite external disturbances will exhibit orbital motions

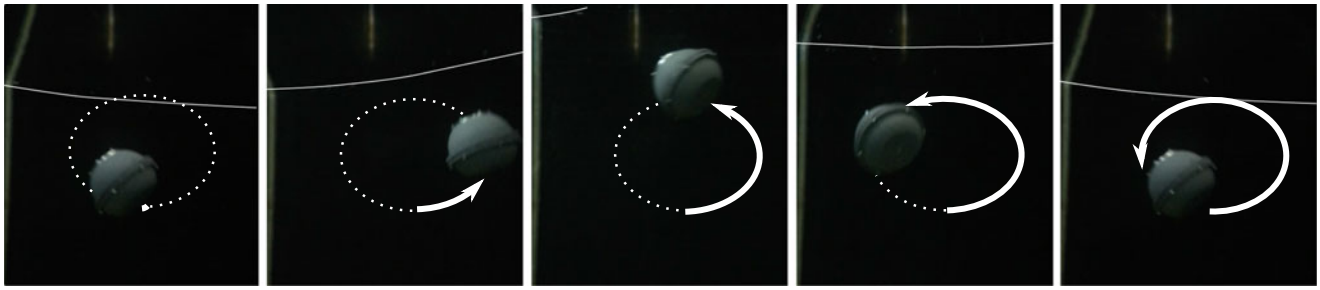

Fig. 11. ADA's orbital motions under wave influence. Subfigures are recorded for progressing time. See attached video for detailed description.

similar to water particles. In a wave tank, ADA is tasked to stabilize itself on an isobar while harmonic water wave trains travel at the surface.

We observe ADA describing elliptical motions at a depth of 25 cm in a wave field of 20 cm wave height, 1.5 s wave period. Screenshots of the motion for five different points in time are shown in Fig. 11. For progressing time the orbital motion shows a slight drift, which is a second order effect in nonlinear wave theory.

It should be noted that, in order to depict a Lagrangian representation of the flow, ADA must be able to match dynamically the density of the surrounding fluid. In fact, as reported by D'Asaro [6], this is the main design challenge for Lagrangian floats. As shown in Fig. 11, the proposed AFFL scheme is able to precisely adjust the required buoyancy, in order to track specific fluid parcels.

V. Conclusion

In this letter we presented ADA and the AFFL depth controller. ADA is an inexpensive diving robot, which was developed as a testbed for depth control research. Given its compact size, it can furthermore serve as a platform for sampling and monitoring of concentrations in industrial tanks. Such applications require precise depth profile tracking. We presented the hardware design and software design of ADA. The software is open-source and the hardware is based on off-the-shelf components. We also introduced the AFFL depth controller and showed in experiments that it outperforms a conventional FL approach in depth holding and depth trajectory tracking experiments. ADA in combination with the AFFL controller allows for precise and robust isobar locking. We demonstrated the performance by letting ADA track orbital motions of water particles under wave influence.

References

[1] J. McMahon and E. Plaku, "Autonomous data collection with limited time for underwater vehicles," *IEEE Robot. Autom. Lett.*, vol. 2, no. 1, pp. 112–119, 2017.

[2] M. Ludvigsen and A. J. Srensen, "Towards integrated autonomous underwater operations for ocean mapping and monitoring," *Annu. Rev. Control*, vol. 42, pp. 145–157, 2016.

[3] D. A. Mindell, *Our Robots, Ourselves: Robotics and the Myths of Autonomy*. New York, NY, USA: Viking, 2015.

[4] R. N. Smith and V. T. Huynh, "Controlling buoyancy-driven profiling floats for applications in ocean observation," *IEEE J. Ocean. Eng.*, vol. 39, no. 3, pp. 571–586, 2014.

[5] D. Roemmich *et al.*, "The Argo program: Observing the global ocean with profiling floats," *Oceanography*, vol. 22, no. 2, pp. 34–43, 2009.

[6] E. A. D'Asaro, "Performance of autonomous Lagrangian floats," *J. Atmos. Ocean. Technol.*, vol. 20, no. 6, pp. 896–911, Jun. 2003. [Online]. Available: http://dx.doi.org/10.1175/1520-0426(2003)020<0896:POALF>2.0.CO;2

[7] C. Detweiler, M. Doniec, I. Vasilescu, and D. Rus, "Autonomous depth adjustment for underwater sensor networks: Design and applications," *IEEE/ASME Trans. Mechatronics*, vol. 17, no. 1, pp. 16–24, Feb. 2012.

[8] R. W. L. Coutinho, A. Boukerche, L. F. M. Vieira, and A. A. F. Loureiro, "Geographic and opportunistic routing for underwater sensor networks," *IEEE Trans. Comput.*, vol. 65, no. 2, pp. 548–561, Feb. 2016.

[9] J. S. Jaffe *et al.*, "A swarm of autonomous miniature underwater robot drifters for exploring submesoscale ocean dynamics," *Nature Commun.*, vol. 8, 2017, Art. no. 14189.

[10] A. Griffiths, A. Dikarev, P. R. Green, B. Lennox, X. Poteau, and S. Watson, "Avexis—Aqua vehicle explorer for in-situ sensing," *IEEE Robot. Autom. Lett.*, vol. 1, no. 1, pp. 282–287, Jan. 2016.

[11] R. M. Sorensen, *Basic Coastal Engineering*, 3rd ed. New York, NY, USA: Springer, 2006.

[12] W. M. Bessa, E. Kreuzer, L. Krumm, M.-A. Pick, and E. Solowjow, "Adaptive fuzzy sliding mode controller and observer for a dive cell," *PAMM*, vol. 15, no. 1, pp. 263–264, 2015.

[13] K. Tanakitkorn, P. A. Wilson, S. R. Turnock, and A. B. Phillips, "Depth control for an over-actuated, hover-capable autonomous underwater vehicle with experimental verification," *Mechatronics*, vol. 41, pp. 67–81, 2017.

[14] J. Higgins and C. Detweiler, "The waterbug sub-surface sampler: Design, control and analysis," in *Proc. 2016 IEEE/RSJ Int. Conf. Intell. Robots Syst.*, Oct. 2016, pp. 330–337.

[15] M. Makrodimitris, I. Aliprantis, and E. Papadopoulos, "Design and implementation of a low cost, pump-based, depth control of a small robotic fish," in *Proc. 2016 IEEE/RSJ Int. Conf. Intell. Robots Syst.*, Sep. 2014, pp. 1127–1132.

[16] B. McGilvray and C. Roman, "Control system performance and efficiency for a mid-depth lagrangian profiling float," *OCEANS 2010 IEEE Sydney*, pp. 1–10, May 2010. [Online]. Available: http://dx.doi.org/10.1109/OCEANSSYD.2010.5603906

[17] W. M. Bessa, M. S. Dutra, and E. Kreuzer, "Depth control of remotely operated underwater vehicles using an adaptive fuzzy sliding mode controller," *Robot. Auton. Syst.*, vol. 56, no. 8, pp. 670–677, 2008.

[18] W. M. Bessa, M. S. Dutra, and E. Kreuzer, "An adaptive fuzzy sliding mode controller for remotely operated underwater vehicles," *Robot. Auton. Syst.*, vol. 58, no. 1, pp. 16–26, 2010.

[19] A. J. Healey and D. Lienard, "Multivariable sliding mode control for autonomous diving and steering of unmanned underwater vehicles," *IEEE J. Ocean. Eng.*, vol. 18, no. 3, pp. 327–339, 1993.

[20] J.-J. E. Slotine, "Sliding controller design for non-linear systems," *Int. J. Control*, vol. 40, no. 2, pp. 421–434, 1984.

[21] J. N. Newman, *Marine Hydrodynamics*. Cambridge, U.K.: MIT Press, 1977.

[22] B. Kosko, "Fuzzy systems as universal approximators," *IEEE Trans. Comput.*, vol. 43, no. 11, pp. 1329–1333, Nov. 1994.

[23] R. E. Bellman, *Adaptive Control Processes: a Guided Tour*. Princeton, NJ, USA: Princeton Univ. Press, 1961.

[24] P. Ioannou and B. Fidan, *Adaptive Control Tutorial*. Philadelphia, PA, USA: SIAM, 2006.

[25] Y. Shtessel, C. Edwards, L. Fridman, and A. Levant, *Sliding Mode Control and Observation*. Basel, Switzerland: Birkäuser, 2014.